Synthesis and Characterization of Fe₃O₄@SiO₂@mesoporous-SiO₂ Materials

Shuiping LI [1, 2] [*]

[1] *College of Civil Science and Engineering, Yangzhou University, No. 198, West Huayang Road, Yangzhou, Jiangsu, 225127, P. R. China*
[2] *Research Institute of Green Building Materials, Yangzhou University, Yangzhou, 225127, P. R. China*

In this work, a magnetic Fe₃O₄@SiO₂@mesoporous-SiO₂ (F@S@m-S) material was successfully prepared by a three-step method: firstly, Fe₃O₄ particles were synthesized through hydro-thermal synthesis process; secondly, Fe₃O₄@SiO₂ materials were fabricated via a template method using tetraethyl orthosilicate (TEOS) as silicon sources and cetyltrimethylammonium chloride (CTAC) as templates; lastly, F@S@m-S materials were prepared through a template method as well. The influence of TEOS/CTAC molar ratio on the morphology and mesostructure was investigated. The product was characterized by Fourier-transform Infrared Spectroscopy (FT-IR), small-angle X-ray scattering (SAXS), scanning electron microscopy (SEM), transmission electron microscope (TEM), and N₂ adsorption-desorption. The results demonstrated that F@S@m-S materials have a well spherical morphology and a typical mesostructure. The increase of TEOS/CTAC molar ratio can improve the mesostructure and crystal form of F@S@m-S materials. The average particle size, specific surface area, average pore size and pore volume of F@S@m-S-4.78 materials are 130 nm, 77.1 m²/g, 9.2 nm and 0.1668 cm²/g, respectively.
Keywords: mesoporous silica, microspheres, TEOS.

1. INTRODUCTION

Transition metal oxides, especially nanoparticles with unique properties owing to finite size effects [1], have attracted much interest in transforming hazardous organic wastes into low toxicity compounds as a catalyst [2]. However, one barrier of this transformation is dependent on the specific surface area and matter transmission channel of carriers, which restrict the contact of transition metal nanoparticles and hazardous organic waste [3 – 6]. Another barrier is the dispersion of transition metal nanoparticles in carriers [3].

In order to overcome these two obstacles, the active transition metal nanoparticles are usually immobilized on the solid carriers such as porous carbon [7] and mesoporous materials [8]. Mesoporous silica, which exhibits a high specific surface area, regularly pore channel, adjustable pore size and tunable pore volume, is an ideal carrier for transition metal nanoparticles [9 – 12]. These excellent characters of mesoporous materials are favorable for well dispersion and prevent the aggregation of transition metal nanoparticles [2].

In the current work, a magnetic Fe₃O₄@SiO₂@mesoporous-SiO₂ (F@S@m-S) material was prepared by a three-step method by using tetraethyl orthosilicate (TEOS) as silica source and cetyltrimethylammonium chloride (CTAC) as templates. The effect of TEOS/CTAC ratio on the morphology and mesostructured was studied. F@S@m-S materials presented a typical mesostructured and uniform spherical morphology.

2. EXPERIMENTAL

2.1. Materials

Ferrous sulfate heptahydrate (FeSO₄·7H₂O, 99.0 %) and sodium acetate (CH₃COONa·3H₂O, 99 %) were supplied by Jiangsu Yixing Second Chemical Reagent Factory. Aqueous ammonia (NH₃·H₂O, 99.0 %), ammonium nitrate (NH₄NO₃, 99.2 %) and triethanolamine (TEA, 99.0 %) were purchased from Jiangsu Tongsheng Chemical Reagent CO., LTD. Sodium dodecylbenzene sulfonate (SDS, 98.5 %) was obtained from Tianjin BASF Chemical Trade Co., LTD. Tetraethyl orthosilicate (TEOS, 99.9 %) and Cetyltrimethylammonium chloride (CTAC, 99.0 %) were supplied by Sinopharm Chemical Reagent Co., LTD. Ethanol (99.0 %) was purchased from Chengdu Kelong Chemical Reagent Co., LTD. All above chemical reagents were used directly without further treatment except when mentioned.

2.2. Synthesis of ferric oxide (Fe₃O₄)

Typically, 1.4 g of FeSO₄·7H₂O, 3.6 g of sodium acetate and 0.5 g of SDS were added successively into 70 mL of deionized water and stirred for 30 min under magnetic stirring at 200 rpm to form a solution. The solution was removed to a Teflon-lined stainless-steel autoclave and kept in vacuum oven at 200 °C for 8 h. After cooling to room temperature, the black precipitates were obtained by centrifugation, washed with ethanol and deionized water for three times, and dried in vacuum at 60 °C for 12 h and then at 105 °C for 4 h. The X-ray diffraction pattern (XRD) of particles was shown in Fig. 1.

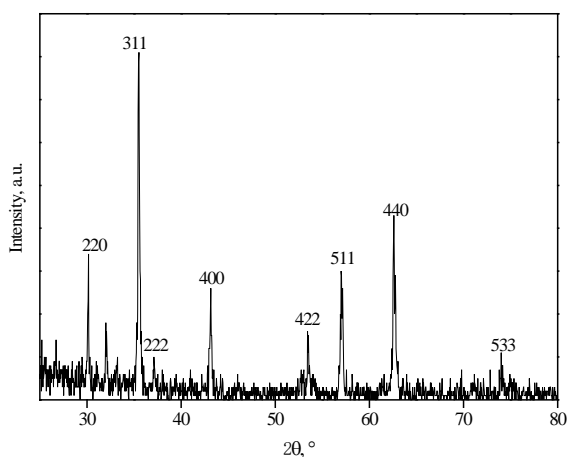[*] Corresponding author. Tel.: +86-514-87979408; fax: +86-514-87979408. E-mail address: *lishuiping2002@hotmail.com* (S. Li)

Fig. 1. The X-ray diffraction pattern (XRD) of particles

2.3. Fabrication of Fe₃O₄@SiO₂

The fabrication of $Fe_3O_4@SiO_2$ materials was performed following the procedure suggested by Sun [2]: 0.2 g of Fe_3O_4 particles were added into 40 mL of ethanol and sonicated at 30 °C for 30 min. Then, 20 mL of deionized water, 40 mL of ethanol and 1 mL of aqueous ammonia were added into the mixture. 0.2 g of TEOS was added and stirred under magnetic stirring at room temperature for 6 h. The gray precipitates were obtained by centrifugation, washed with ethanol and deionized water for three times and dried in vacuum at 60 °C for 12 h and then at 105 °C for 4 h.

2.4. Preparation of Fe₃O₄@SiO₂@mesoporous-SiO₂

Deionized water, 24 mL of CTAC and 0.18 g of TEA were added into a 250 mL three-neck round-bottomed flask equipped with a thermometer, a constant-voltage dropping funnel, and a condenser pipe. 0.2 g of $Fe_3O_4@SiO_2$ particles were added into the solution and sonicated for 1 h, followed by stirring at 60 °C for 1 h under magnetic stirring at 300 rpm. Appropriate amount of TEOS was dropwise into the solution and stirred at 60 °C for 12 h under reflux conditions. The precipitates were obtained by centrifugation, washed with ethanol and deionized water for three times, and dried in vacuum at 80 °C for 4 h and then at 105 °C for 6 h. The final products (F@S@m-S-x), where x denotes the molar ratio of TEOS/CTAC (4.58, 4.78 and 4.98), were removed to a muffle furnace and heated to 600 °C with a speed of 1 °C/min and calcined for 6 h.

2.5. Characterization

Fourier-transform Infrared Spectroscopy (FT-IR) spectra were measured with a Tensor 37 instrument (Germany, Bruker) through Potassium bromide pellet method. Each sample was scanned in the range of 600-1800 cm^{-1} with a resolution of 4 cm^{-1}.

Small-angle X-ray scattering (SAXS) patterns were recorded on a X'Pert₃ Powder (PANalytical, Netherlands) using Cu Kα radiation.

Scanning electron microscopy (SEM) images were recorded using a scanning electron microscope (Hitachi SU8000), and the samples were sputter-coated with gold before observation. SEM micrographs were obtained under conventional secondary electron imaging conditions with an accelerating voltage of 10 kV.

Transmission electron microscope (TEM) morphologies were observed by a JEM-2100F (JEOL, Japan) with an accelerating voltage of 200 kV, matching with a X-MaxN 80T IE250 energy dispersive spectrometer (EDS). Powder samples were suspended in ethanol using an ultrasonic horn and small volumes of the suspensions were deposited onto carbon-coated 400 mesh copper grids and dried under air.

N_2 adsorption-desorption isotherms at 77 K were measured with a Tristar II 3020 instrument (Micromeritics, USA). The specific surface area was calculated by the Brunauer-Emmett-Teller (BET) method from the linear part of BET plot according to IUPAC recommendations using the adsorption isotherm (relative pressure $(P/P_0) = 0.05 - 0.20$). The pore size distribution and pore volume were calculated by the Barrett-Joyner-Halenda (BJH) method.

3. RESULTS AND DISCUSSION

The FT-IR spectrum of $Fe_3O_4@SiO_2$ materials is shown in Fig. 2. The vibration band at 587 cm^{-1} is assigned to stretching vibration of Fe-O, which indicates the presence of Fe_3O_4. The vibration band at 1092 cm^{-1} is attributed to asymmetric stretching vibration of Si-O-Si, which results from the hydrolysis of TEOS. The appearance of vibration band at 1092 cm^{-1} indicates the successful coating with SiO_2 on the surface of Fe_3O_4 materials. However, this spectrum demonstrates that Fe_3O_4 particles have not been totally covered by SiO_2 particles.
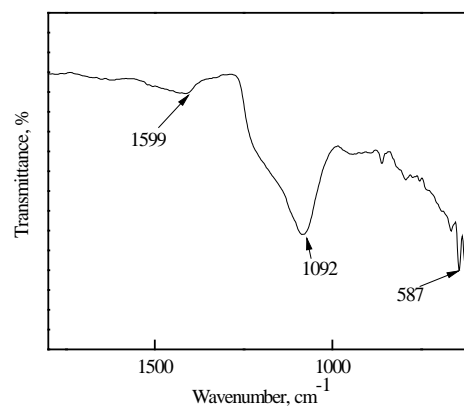

Fig. 2. FT-IR spectrum of Fe₃O₄@SiO₂ materials

The FT-IR spectra of F@S@m-S materials are shown in Fig. 3. The vibration bands at 651.4, 798.2 and 1085.2 cm^{-1} are assigned to asymmetric stretching vibration of Si-O, symmetric stretching vibration of tetrahedral SiO_4 unit and asymmetric stretching vibration of Si-O-Si, respectively. The bands at 1085.2 cm^{-1} in the spectra of F@S@m-S-4.78 and F@S@m-S-4.98 are clearer than that in F@S@m-S-4.58. These results indicate that the increase of TEOS/CTAC molar ratio is beneficial to the formation of F@S@m-S materials.

The SAXS patterns of F@S@m-S materials are shown in Fig. 4. The SAXS pattern of F@S@m-S-4.58, (Fig. 4 a) presents two weak diffraction peaks at $2\theta = 0.86°$ and $2\theta = 1.72°$, which can be indexed to the 100 and 110 planes of mesostructures, respectively.
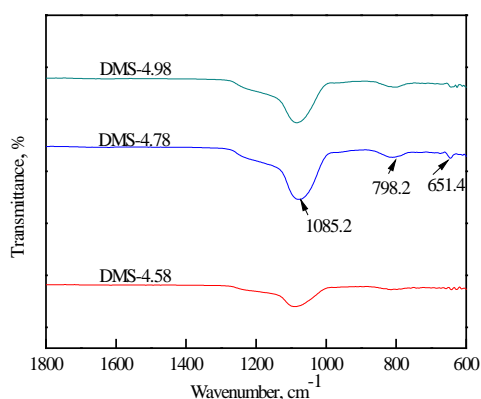
Fig. 3. FT-IR spectra of DMS-x materials

The unit cell parameter is calculated to be about 11 nm. These two characteristic peaks suggest that F@S@m-S-4.58 materials have mesoporous structure [13]. The SAXS pattern of F@S@m-S-4.78 (Fig. 4 b) shows a strong diffraction peak at $2\theta = 0.86°$ and a weak diffraction peak at $2\theta = 1.72°$. This result indicates that increasing TEOS/CTAC molar ratio can improve the mesostructured state and influence the crystal form of F@S@m-S materials.
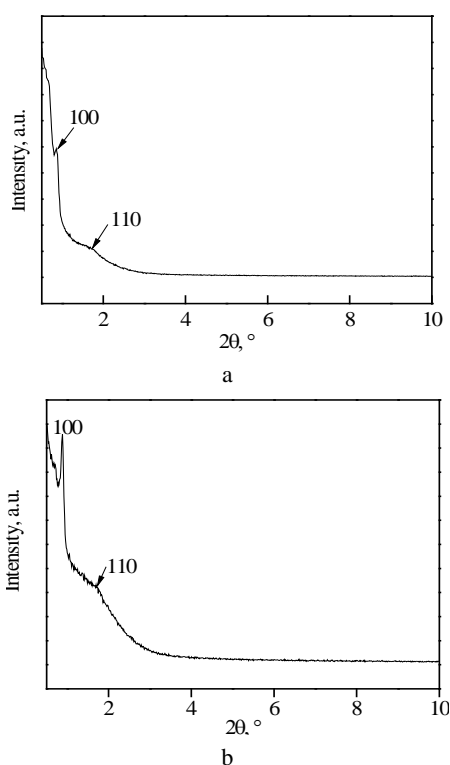

Fig. 4. SAXS patterns: a – DMS-4.58; b – DMS-4.78

SEM images of F@S@m-S materials are presented in Fig. 5. As shown in Fig. 5, all F@S@m-S materials exhibit a spherical morphology. F@S@m-S-4.58, F@S@m-S-4.78 and F@S@M-S-4.98 materials have an average particle sizes of 100 nm, 130 nm and 180 nm, respectively. The increase of TEOS/CTAC molar ratio, which supplies enough silicon sources, can increase the particle sizes of F@S@m-S materials. This result indicates that a higher TEOS/CTAC molar ratio can be beneficial to obtaining F@S@M-S materials with bigger particle size.
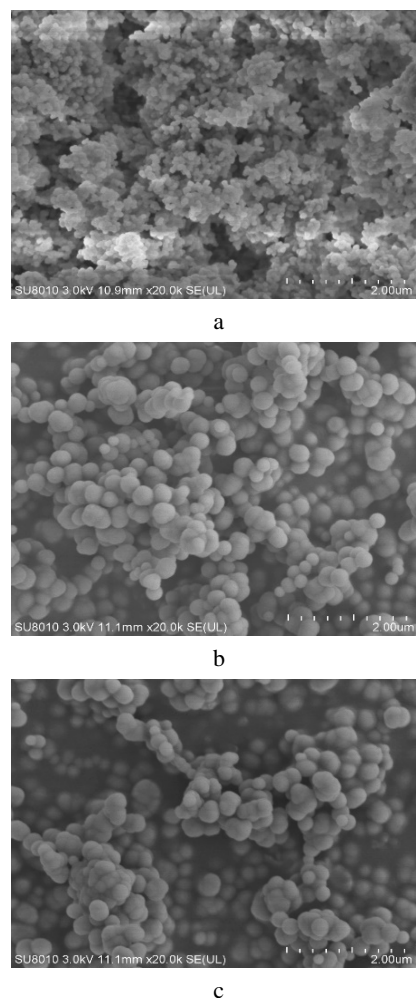

Fig. 5. SEM images: a – DMS-4.58; b – DMS-4.78 (B); c – DMS-4.98

TEM morphologies of F@S@m-S materials of F@S@m-S-4.78 materials are shown in Fig. 6. As shown in Fig. 5 a, F@S@m-S-4.78 materials present an average size of 130 nm, which is in correspondence with the result observed in Fig. 5. Moreover, F@S@m-S-4.78 materials have well uniform spherical morphology. It can be observed that F@S@m-S-4.78 materials have both ordered and disordered mesoporous structure (Fig. 6 b and c). Disordered mesoporous structure may results in a low specific surface area.

The energy dispersive spectroscopic (EDS) analysis was utilized to determine the chemical composition of the F@S@m-S-4.78 materials and the result are shown in Fig. 6. Fig. 7 shows that the F@S@m-S-4.78 materials present a spectrum containing a signal of C, O, Cu, and Si elements. Among these, the signal of C, O, and Cu were usually affected by the cooper grids and their degree of oxidation. Si and O signals resulted from the F@S@m-S-4.78 materials. It should be noted that there is no signal of Fe element, which demonstrates that Fe_3O_4 was completely coated with mesoporous silica.

N_2 adsorption-desorption method is a typical process for charactering the mesostructure of mesoporous materials. The N_2 adsorption-desorption isotherm of F@S@m-S-4.78 materials is shown in Fig. 8.
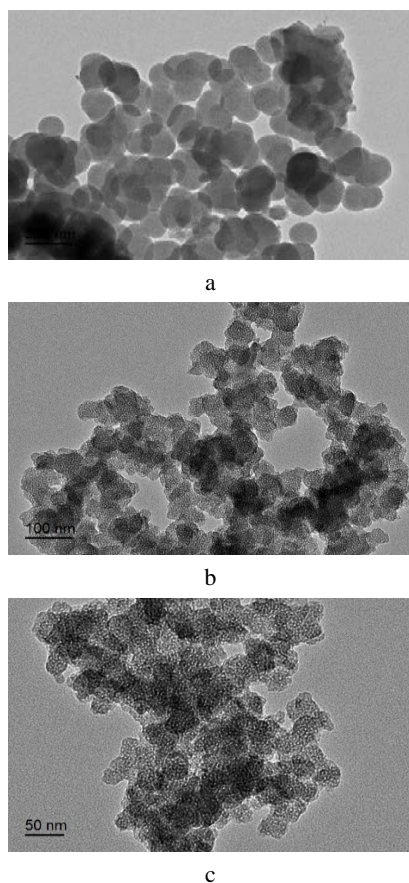
Fig. 6. TEM images of F@S@M-S-4.78 materials: a – 30k X; b – 40k X; c – 50k X
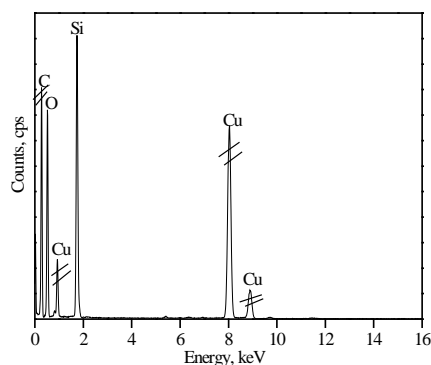

Fig. 7. EDS spectrum of F@S@M-S-4.78 materials
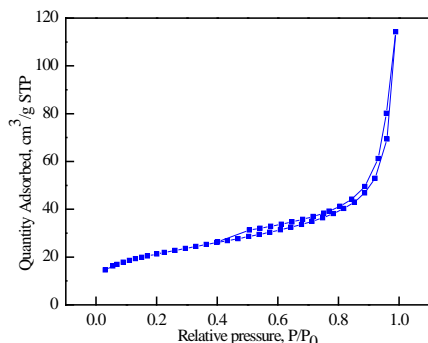

Fig. 8. The N_2 adsorption-desorption isotherm of F@S@M-S-4.78 materials

It can be seen that the isotherm of F@S@m-S-4.78 materials is a type-IV curve with long and narrow hysteresis

loop, which indicates the existence of mesopores and results from capillary condensation in mesopores [14]. The specific surface area, average pore size and pore volume of F@S@m-S-4.78 materials are calculated to be 77.1 m^2/g, 9.2 nm and 0.1668 cm^2/g, respectively. It is well known that the specific surface area of ordered mesoporous materials is higher than that of mesoporous materials with disordered mesoporous structure. The low specific surface area of this materials may be attributed to the disordered mesoporous structure which is observed in Fig. 6.

4. CONCLUSIONS

In summary, Fe_3O_4@SiO_2@mesoporous-SiO_2 (F@S@m-S) materials were successful prepared by a three-step method, using Ferrous sulfate heptahydrate as iron source, TEOS as silica source, SDS and CTAC as templates. The effect of TEOS/CTAC molar ratio on the morphology and mesostructured was investigated. The products were characterized by FT-IR, SAXS, SEM, TEM and N_2 adsorption-desorption. F@S@m-S materials present a uniform spherical morphology and exhibit a typical mesoporous structure. The increase of TEOS/CTAC molar ratio may improve the mesostructured state. The three-step method provides a cost-effective procedure for the preparation of magnetic Fe_3O_4@SiO_2@mesoporous-SiO_2 materials with uniform spherical morphology.

REFERENCES

1. **Gross, A.F., Diehl, M.R., Beverly, K.C., Richman, E., Tolbert, S.H.** Controlling Magnetic Coupling between Cobalt Nanoparticles through Nanoscale Confinement in Hexagonal Mesoporous Silica *The Journal of Physical Chemistry B* 107 (23) 2003: pp. 5475 – 5482. https://doi.org/10.1021/jp034240n

2. **Sun, Z.B., Li, H.Z., Cui, G.J., Tian, Y.X., Yan, S.Q.** Multifunctional Magnetic Core-Shell Dendritic Mesoporous Silica Nanospheres Decorated with Tiny Ag Nanoparticles as a Highly Active Heterogeneous Catalyst *Applied Surface Science* 360 2016: pp. 252 – 262. https://doi.org/10.1016/j.apsusc.2015.11.013

3. **Han, Y.F., Chen, F.X., Zhong, Z.Y., Ramesh, K., Chen, L.W., Widjaja, E.** Controlled Synthesis, Characterization, and Catalytic Properties of Mn_2O_3 and Mn_3O_4 Nanoparticles Supported on Mesoporous Silica SBA-15 *The Journal of Physical Chemistry B* 110 (48) 2006: pp. 24450 – 24456. https://doi.org/10.1021/jp064941v

4. **Li, Z.Y., Liu, Y., Wang, X.Q., Liu, L.H., Hu, J.J., Luo, G.F., Chen, W.H., Rong, L.F., Zhang, X.Z.** One-Pot Construction of Functional Mesoporous Silica Nanoparticles for the Tumor-Acidity-Activated Synergistic Chemotherapy of Glioblastoma *ACS Applied Materials & Interfaces* 5 (16) 2013: pp. 7995 – 8001. https:// doi.org/10.1021/am402082d

5. **Li, W., Wang, F., Liu, Y.P., Wang, J.X., Yang, J.P., Zhang, L.J., Elzatahry, A.A., Al-Dahyan, D., Xia, Y.Y., Zhao, D.Y.** General Strategy to Synthesize Uniform Mesoporous TiO_2/Graphene/Mesoporous TiO_2 Sandwich-Like Nanosheets for Highly Reversible Lithium Storage *Nano Letters* 15 (3) 2015: pp. 2186 – 2193. https://doi.org/10.1021/acs.nanolett.5b00291

6. **Liu, Y., Lan, K., Bagabas, A.A., Zhang, P.F., Gao, W.J., Wang, J.X., Sun, Z.K., Fan, J.W., Elzatahry, A., Zhao, D.Y.** Ordered Macro/Mesoporous TiO_2 Hollow Microspheres with Highly Crystalline Thin Shells for High-Efficiency Photoconversion *Small* 12 (7) 2016: pp. 860 – 867. https://doi.org/10.1002/smll.201503420

7. **Fang, Y., Wang, E.** Simple and Direct Synthesis of Oxygenous Carbon Supported Palladium Nanoparticles with High Catalytic Activity *Nanoscale* 5 (5) 2013: pp. 1843 – 1848. https://doi.org/10.1039/c3nr34004j

8. **Alamri, H., Noémie, B., Jérôme, L., Guari, Y., Larionova, J., Kleinke, K., Kleinke, H., Prouzet, E.** Integrative Synthesis of Coordination Polymers, Metal Oxides, and Alloys Magnetic Nanoparticles in MSU Mesoporous Silica *Chemistry of Materials* 26 (2) 2014: pp. 875 – 885. https://doi.org/10.1021/cm4001625

9. **Zaccariello, G., Back, M., Zanello, M., Canton, P., Cattaruzza, E., Riello, P., Alimonti, A.** Formation and Controlled Growth of Bismuth Titanate Phases into Mesoporous Silica Nanoparticles: An Efficient Self-Sealing Nanosystem for UV Filtering in Cosmetic Formulation *ACS Applied Materials & Interfaces* 9 (2) 2017: pp. 1913 – 1921. https://doi.org/10.1021/acsami.6b13252

10. **Zhang, S.H., Wen, L., Yang, J.P., Zeng, J.F., Sun, Q., Li, Z., Zhao, D.Y., Dou, S.X.** Facile Fabrication of Dendritic Mesoporous SiO_2@CdTe@SiO_2 Fluorescent Nanoparticles for Bioimaging *Particle & Particle Systems Characterization* 33 (5) 2016: pp. 261 – 270. https://doi.org/10.1002/ppsc.201500254

11. **Huang, W.Y., Zink, J.I.** Effect of Pore Wall Charge and Probe Molecule Size on Molecular Motion inside of Mesoporous Silica Nanoparticles *The Journal of Physical Chemistry C* 120 (41) 2016: pp. 23780 – 23787. https://doi.org/10.1021/acs.jpcc.6b06293

12. **Tajiri, T., Saisho, S., Mito, M., Deguchi, H., Konishi, K., Kohno, A.** Size Dependence of Crystal Structure and Magnetic Properties of NiO Nanoparticles in Mesoporous Silica *The Journal of Physical Chemistry C* 119 (2) 2015: pp. 1194 – 1200. https://doi.org/10.1021/jp5112372

13. **Rojas, F., Kornhauser, I., Felipe, C., Esparza, J.M., Cordero, S., Domínguez, A., Riccardo, J.L.** Capillary Condensation in Heterogeneous Mesoporous Networks Consisting of Variable Connectivity and Pore-size Correlation *Physical Chemistry Chemical Physics* 4 (11) 2002: pp. 2346 – 2355. https://doi.org/10.1039/B108785A

14. **Wang, J.X., Feng, S.S., Song, Y.F., Li, W., Gao, W.J., Elzatahry, A.A., Aldhayan, D., Xia, Y.Y., Zhao, D.Y.** Synthesis of Hierarchically Porous Carbon Spheres with Yolk-shell Structure for High Performance Supercapacitors *Catalysis Today* 243 2015: pp. 199 – 208. https://doi.org/10.1016/j.cattod.2014.08.037